Corrosion Science 50 (2008) 2779–2784

Contents lists available at ScienceDirect

Corrosion Science

journal homepage: www.elsevier.com/locate/corsci

Nano-pit corrosion of the tabs in aluminum electrolytic capacitor: Polarization characteristics of the tabs in ethyleneglycol–borate solution with chloride ions

Rong Xue, Yuan-Yuan Qian, Ke-Ke Liu, Xiao-Xing Jiang, Jun-Jie Zhu, Jian-Rong Zhang *

Key Lab of Analytical Chemistry for Life Science, School of Chemistry and Chemical Engineering, Nanjing University, Nanjing 210093, China

ARTICLE INFO

Article history:
Received 30 January 2008
Accepted 27 July 2008
Available online 6 August 2008

Keywords:
A. Aluminum
B. AFM
B. Polarization
C. Pitting corrosion

ABSTRACT

To evaluate the corrosion behavior of the anode tab in aluminum electrolytic capacitor, we performed some electrochemical and morphology analysis using the polarization curves in conjunction with atomic force microscope (AFM), scanning electronic microscope (SEM) and optical microscope (OM). The results suggest that the current oscillation was found to be associated with nano-pit, which is defined as the rectangular pit (β) with a depth less than 55 nm and a width no more than 100 nm. Furthermore, elevation of Cl^- concentration widened the crevices caused by electrolytic tension, enlarged the nano-pit area, and accelerated the electrochemical reaction rate of the anode tab in ethyleneglycol–borate solution. These findings may have implications for the failure of aluminum electrolytic capacitor.

1. Introduction

Although such new capacitors as double-layer capacitors, pseudocapacitors, hybrid capacitors and multi-layer ceramic chip capacitors have been developed over the past few decades [1–3], aluminum electrolytic capacitor is still a kind of electronic element which is widely used with great demand owing to its very high capacitance, wide working potential range with an excellent price/performance ratio [1]. Among the aluminum electrolytic capacitors one with multi-tabbing of the foil windings is shown in Fig. 1, which is constructed of the aluminum anode foil that is coated with an oxide dielectric, an organic solution to provide electrical continuity, a porous papers to hold the electrolyte, and a cathode foil to serve as a current collector.

While such aluminum electrolytic capacitors have been widely used in electronics industry [1], some problems are presented during their working life such as anodic corrosion on the anode foil and the anode tab. The anodic corrosion attributes to the negative consequences of aluminum electrolytic capacitor, for example, shortening the service life and premature failure. The failure is significantly caused by the electrochemical corrosion of the anode tab or the rivet (a component connecting the anode tab and the cover in aluminum electrolytic capacitor) by analyzing a batch of failure products. This phenomenon is prevalent in aluminum electrolytic capacitors used at relatively high voltage, especially above 400 V. The resistance to corrosion of the anode tabs is lower than that of the anode foil, for the thickness of the oxide film on the anode tab is thinner than that on anode foil. Therefore, the anode tab is apt to be corroded.

Generally, the anodic failure can be caused by halogenated solvents [2] and the quality of the elements such as the aluminum foil, the electrolytic paper, and the cover [3]. Consequently, some models were proposed to predict the life time or the failure of aluminum electrolytic capacitor [4–11]. However, the information on the anode tab corrosion is still lacking except for the methods of anticorrosion on the aluminum tabs [12], the tab corrosion caused by the electrolytic decomposition products [13], and the detection of the critical Cl^- concentration by leakage currents [14]. Relatively little attention has been paid to the corrosion on the anode tab of aluminum electrolytic capacitor used at high voltage above 400 V.

The present work is therefore to evaluate, understand and discuss the mechanism of the anodic corrosion of the anode tab, which is used in aluminum electrolytic capacitor at high voltage of 400 V, in ethyleneglycol–borate solutions with chloride ions. The corrosion of the anode tab was investigated by polarization curves combined with atomic force microscope (AFM), scanning electronic microscope (SEM) and optical microscope (OM) measurements. We satisfactorily explained the relationship between the current oscillation, the nano-pits and the concentration of Cl^- ions, and obtained the electrochemical parameters for the anode tab as a function of chloride-ion concentration by fitting at the same time.

* Corresponding author. Tel.: +86 25 83686130; fax: +86 25 83317761.
E-mail address: jrzhang@nju.edu.cn (J.-R. Zhang).

0010-938X/$ - see front matter © 2008 Elsevier Ltd. All rights reserved.
doi:10.1016/j.corsci.2008.07.021

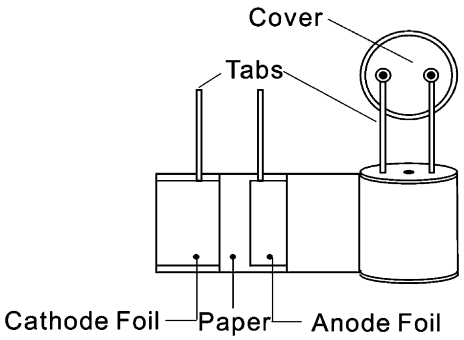

Fig. 1. Schematic of the aluminum (Al) electrolytic capacitor.

2. Experimental

2.1. Samples and solutions

The electrodes were made of a sheet of aluminum anode tab (99.99%, 200 μm thick) and cathode tab (99.85%, 200 μm thick) used in aluminum electrolytic capacitor for high voltage of 400 V (supplied by Japan Capacitor Industrial Co., Ltd, and the chemical composition (wt.%) of the aluminum anode tab is presented in Table 1). The specimen were embedded in silicone manufactured by Kangda chemical factory (Liyang, Jiangsu China) resulting in an exposed aluminum area of 1.2 cm^2. The working surfaces were cleaned by distilled water and acetone prior to testing.

The working solution (supplied by Jianghai Capacitor Co., Ltd), which is used for the aluminum electrolytic capacitors applied at the voltage of 400 V, is mainly constructed by ethyleneglycol–borate system. All solutions with Cl^- were made from analytical grade reagent of sodium chloride.

2.2. Anodizing

Firstly, the oxide films were formed on the anode tab using a TV Meter (YTV-51A, Yangzhou Shuanghong Ltd., China) in the working solution with or without Cl^- ions at 80 °C, initially galvanostatically at anodic current of 1 mA cm^{-2} up to a certain anodic voltage (the anodic voltage which leveled off under 1 mA cm^2 is 400 V for the solution with free, 2 ppm and 5 ppm Cl^- ion, 110 V and 6 V for the solution containing 50 ppm and 1000 ppm Cl^- ion, respectively). An aluminum anode tab was used as an anode electrode, and an aluminum cathode tab was used as a cathode electrode. A certain thickness of oxide film on the anode tab is formed when the leakage current is leveled off at potentiostatic anodizing.

2.3. Polarization measurements

Aluminum anode tabs anodized potentiostatically were immerged in ethyleneglycol–borate solution with free or different concentrations of Cl^- at 80 °C, and the polarization curves were measured by changing the electrode potential automatically from −1.2 to 2.2 V with scanning rate of 0.5 mV s^{-1}. The aluminum anode tab working electrode (WE) was tested in a conventional three-electrode electrochemical cell. An Ag/AgCl/3.5 M KCl reference electrode (RE) was connected to the cell through a Luggin capillary. A platinum was used here as the counter electrode (CE). The electrochemical measurements were performed with an Autolab potentiostat/galvanostat/frequency_response_analyzer (Ecochemie), PGSTAT30/FRA2, controlled by the GPES/FRA v.4.9.5 software. The cell was a water-jacketed version, connected to a constant temperature circulator.

2.4. Morphology measurements

The corrosion morphology was observed by atomic force microscope (AFM), scanning electronic microscope (SEM) and optical microscope (OM) measurements. AFM was carried out on an SPA 300HV SPM scanning probe microscope, OM was carried out on a Nikon eclipse TE2000-U microscope, and the morphologies of the anode tabs were measured using a JSM scanning electron microscope (SEM). Before SEM measurement, the samples were sputtered with thin layers of platinum.

FemtoScan™ online software (advanced technologies center, http://www.nanoscopy.net) were used to process the surface roughness, data of AFM, and the crevice width in OM. Measurement of pit densities was made simpler through the use of image analysis software called scion image (http://www.scioncorp.com).

3. Results and discussion

3.1. Effect of chloride ions on the nano-pit

A chloride ion-dependent change of the anode-tab surface morphology is observed after anodized potentiostatically in the solution with various concentrations of chloride ions by the series of AFM images (Fig. 2), where the particles are an oxide film with a composition close to Al_2O_3 indicated by Auger spectra [15]. It can be seen that the morphology of the high-roughness areas depends on the concentration of chloride ions. Surface topographical data can be obtained in two dimensions, i.e. $z(x, y)$. The data can be processed and then the surface roughness parameters obtained. The root mean-square surface roughness (R_q) was calculated as follows [16]:

$$R_q = \sqrt{\frac{1}{n}\sum_{i=1}^{n} z_i^2} \quad (1)$$

where z_i is the height or depth of the ith highest or lowest deviation and n is the number of discrete profile deviations. As an example of surface roughness progressions, Table 2 shows the calculated roughness vs. concentration of Cl^- ions acting on the aluminum anode tabs.

Two different types of pits are observed (marked by arrows and illustrated by cross-sections in Fig. 2), namely line-shaped pits (α) and rectangular pits (β) for all anode tabs anodized potentiostatically with various concentrations of Cl^-. In the following we will first give an overview of the anode-tab morphology with various Cl^- concentrations and then discuss the various morphological features in detail.

The formation of various types of smaller pits with surface areas of 3.5×10^3–1.0×10^4 nm^2 is observed on AFM images (Fig. 2a) after anodized potentiostatically in the solution with free chloride

Table 1
Chemical composition (wt.%) of the aluminum anode tab and aluminum cathode tab

Electrodes	Al	Si	Fe	Cu	Mg	Ca	Zn
Aluminum anode tab (+IN 99)	99.99	0.0010	0.0007	0.0033	0.0001	0.0000	0.0065
Aluminum cathode tab (−IN 30)	99.85	0.0400	0.0500	0.0180	0.0020	0.0100	0.0300

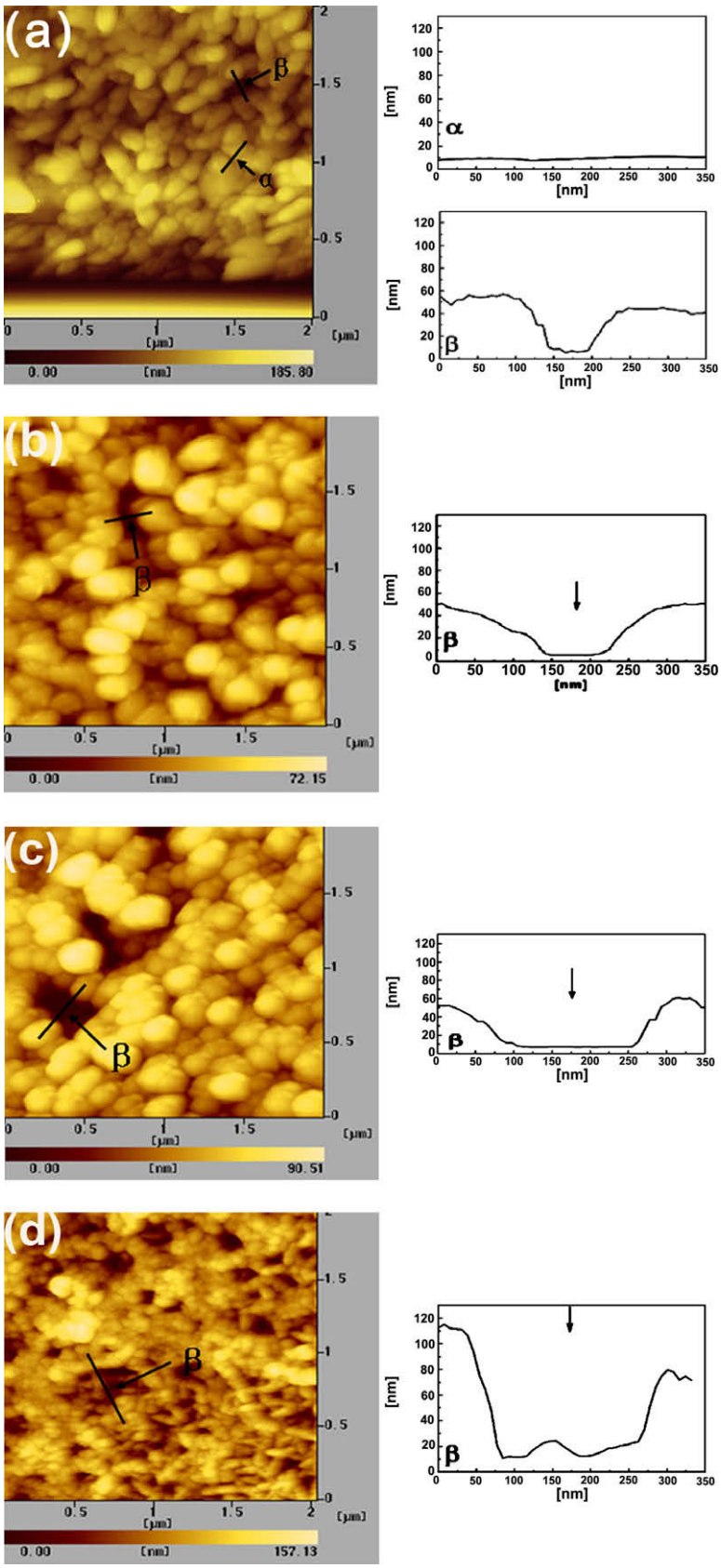

Fig. 2. AFM images ($2 \times 2\ \mu m^2$) of aluminum tabs anodized potentiostatically in the solution with chloride ions of (a) 0 ppm, (b) 2 ppm, (c) 50 ppm and (d) 1000 ppm. Examples of the different types of pits are marked with arrows in the images and illustrated by cross-sections.

ions. The line-shaped pits (α) are usually <10 nm deep and have widths (full width at half maximum in the cross-sections of Fig. 2) of about 20 nm. The other type of observed structures is rectangular pits (β) with sharper edges. The rectangular pits (β)

Table 2
Surfaces roughness as a function of concentrations of solutions with Cl^- ions

C_{Cl^-}/ppm	0	2	50	1000
Roughness/nm	4.64	5.18	5.27	7.16

in this case were less than 50 nm depth and 90 nm width. These pits in surface oxide films provide sites within which anodic dissolution of the metal substrate commences [17]. The pits densities, however, are significant different on the anode tabs with various concentrations of chloride ions. On the sample with free chloride ions, the dominant type of etch pits are the line pits (α) with a saturation density $\approx 3.05 \times 10^9$ cm^{-2} (Fig. 3).

The anode tab in the solution containing 2 ppm Cl^- had the less number of line-shaped pits (α) (Fig. 3) and the wider rectangular pits (β) (examples marked by arrows in Fig. 2b with the width about 99 nm) than that in the solution without Cl^-. While 2 ppm Cl^- ions were added in the solution, the depth of the rectangular pits (β) changed slightly (Fig. 2a and b). Providing that 50 nm is the lower limit of the depth of pits found after millisecond etching [18], we define the nano-pit as those rectangular pits (β) with a depth less than 55 nm and a width no more than 100 nm. Consequently, although the addition of 2 ppm Cl^- widened the pit, the rectangular pits (β) in this case possessed identical characteristics of that without Cl^-, which is defined as the nano-pit previously.

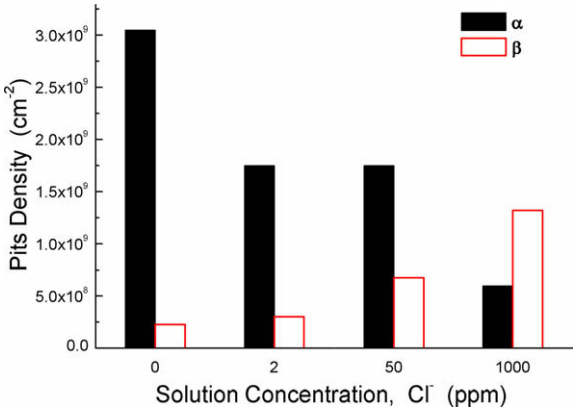

Fig. 3. Dependence of the pits density on Cl^- concentration in ethyleglycol–borate solution.

The oxide layer of the aluminum anode tab was corroded to form larger, isolated, square or rectangular etch pits (Fig. 2c) when the anode tab was anodized potentiostatically in the solution with 50 ppm Cl^-. Also, the enhancement the pits density of rectangular pits (β) (Fig. 3) is ascribed to the enhanced stability of voids upon exposure by chloride ions, since near-surface voids function as sites for corrosion pits [19]. These isolated pits are attributed to nano-pits nucleation at small defects, which can be illustrated in the rectangular pit (β) (marked by arrows in Fig. 2c) with the depth of 60 nm and width of 239 nm. The rectangular pit (β) in this situation is obviously out of the range of nano-pit.

The whole anode-tab surface was covered with the rough etch morphology (Fig. 2d) under anodized potentiostatically in the solution containing 1000 ppm Cl^-. The morphology exhibited an increased density of clusters, consisting of several square/rectangular etch pits. These clusters are probably formed by (anisotropic) lateral growth of the pits and by coalescence of adjacent nano-pits. These clusters led to large rectangular structure with depth >70 nm, width of 250 nm (marked by arrows in Fig. 2d) which were out of the range of nano-pit. Once an oxide layer has been removed by corrosion, the stable passive layer does not readily reform in the presence of chloride ions [17]. Hence the line-shaped pits, which are frequently found on sample with free chloride ions, are reduced dramatically on the sample with 1000 ppm Cl^- (Fig. 3).

These morphological differences among the anode tab anodized potentiostatically in the solution containing various concentrations of Cl^- may be related to the disappearance of most particles on the aluminum surface, which is responsible for the larger pits and the

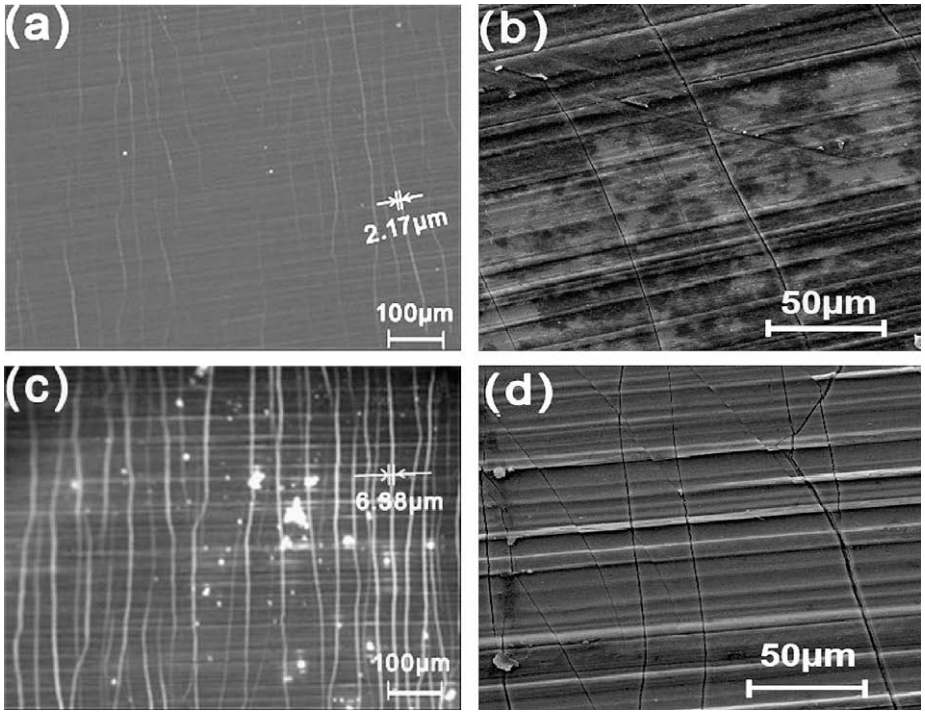

Fig. 4. OM images (a and c) and SEM images (b and d) of aluminum tabs anodized potentiostatically after the anodic polarization in the ethyeneglycol–borate solution with chloride ions of 0 ppm(a and b) and 2 ppm (c and d).

thinner thickness of oxide film by the anodic dissolution. As it has been pointed out by López et al. [20], corrosion appears generally in the form of pitting and the number and size of pits increases with the thickness of the anodic film decreases.

The OM (Fig. 4 a and c) and SEM (Fig. 4c and d) images present the newly formed oxide film obtained after the anodic polarization in the solution with free and 2 ppm Cl^- ion, respectively. These images exhibit characteristic ridges parallel to the rolling direction, which are attributed to the rolling process. In comparing with the oxide film anodized in the solution with and without Cl^-, the crevices nearly perpendicular to the rolling direction on the oxide film were wider and some new crevices were formed after the anodic polarization curves (Fig. 4c and d). More Cl^- ions made the crevice density increase from 3400 cm^{-2} (Fig. 4a) to 4700 cm^{-2} (Fig. 4c) and the crevice average width increased form 3.8 μm (Fig. 4a) to 5.7 μm (Fig. 4c). The new crevice, which becomes the defect of the oxide film, may be attributed to the electric tension on the oxide film by varying anodic potential.

3.2. Effect of chloride ions on the polarization characteristic

Fig. 5 illustrates the influence of chloride ions on the aluminum-tab polarization curves in the ethyleneglycol–borate solution. Corrosion potential ($\boldsymbol{E}_{corr}$), corrosion current density ($\boldsymbol{I}_{corr}$), and anodic/cathodic Tafel constant (b_a and b_c) were derived from these data. Based on the approximately linear polarization behavior near open-circuit potential (OCP) (around ±10 mV), the polarization resistance ($\boldsymbol{R}_p$) values were determined from Stern–Geary equation [21]:

$$\mathbf{R}_p = \frac{b_a b_c}{2.303 I_{corr}(b_a + b_c)} \tag{2}$$

Results of potentiodynamic polarization were summed in Table 3.

These data clearly show that the corrosion resistance of the anode tab with various Cl^- ion concentrations was evidently different. In contrast to those with free Cl^- ions, the anode tabs with Cl^- ions all had more negative corrosion potential, much higher corrosion current density and much lower polarization resistance, suggesting an increase in the charge carrier density within the oxide film [22]. The polarization curves of the anode tab with Cl^- had relatively lower Tafel slope due to the film thinner in thickness [23] and with more micro-defects than those with free Cl^- ions. This indicates that the corrosion resistance of the anode tab is damaged obviously with more Cl^- ions.

Table 3
Electrochemical parameters of anode tabs as a function of chloride-ion concentration

Cl^- concentration/ppm	b_a/V dec^{-1}	b_c/V dec^{-1}	$\boldsymbol{E}_{corr}$/V	$\boldsymbol{I}_{corr}$/A cm^{-2}	$\boldsymbol{R}_p$/Ω
0	0.328	0.115	−0.447	8.50×10^{-11}	4.20×10^{8}
2	0.232	0.113	−0.457	7.34×10^{-10}	4.50×10^{7}
5	0.113	0.097	−0.467	9.27×10^{-10}	2.44×10^{7}
50	0.077	0.095	−0.505	1.08×10^{-8}	1.71×10^{6}
1000	0.043	0.087	−0.596	1.32×10^{-8}	9.47×10^{5}

Inspection the data in Table 3 reveals that an increase of Cl^- concentration shifts $\boldsymbol{E}_{corr}$ towards more negative direction. From these results, reasonable linear $\boldsymbol{E}_{corr}$ vs. $\log C_{Cl^-}$ is obtained in Fig. 6. The least-square fit for the curve corresponds to:

$$\mathbf{E}_{corr} = -0.43 \log C_{cr^-} + (-0.052) \tag{3}$$

which is consistent with the form of the corrosion potential as a function of halide activity [24].

Different polarization behavior is also significant in the samples containing various Cl^- concentrations (Fig. 5) except the more negative corrosion potential, higher corrosion current density and lower polarization resistance compared with free Cl^-. This difference can be observed especially in the anodic branch of potentiodynamic polarization curves (Fig. 5) which represent current oscillations in the solution containing chloride ions less than or equal to 2 ppm (Fig. 5a and b) while no oscillation is observed in the solution with Cl^- ions more than 5 ppm (c–e in Fig. 5).

The oscillations in the current from several hundred milivolts above the corrosion potential ($\boldsymbol{E}_{corr}$) appeared in the anodic polarization curves at low Cl^- concentrations (⩽2 ppm). These oscillations are attributed to the consecutive formation and the self-healing of the surface defects such as line-shaped pits (α) (Fig. 2a) and nano-pits (rectangular pits (β) in Fig. 2a and b), which are very small in size and are compensated automatically during the anodization [25]. These compensated nano-defects and nano-pits are the same as the consecutive formation and repassivation of metastable pits [26,27], which has been shown previously by Pistorius and Burstein [28] that the current first increases as the pits nucleate and grow then decreases after a short time with the occurrence of the metastable pits. The current increases first, then decreases with the occurrence of the nano-pits. The elevation of the current is attributed to the anodic oxidation reaction processes, and the reduction of the current is due to the self-healing of aluminum as a valve-metal. Moreover, the Al^{3+} ions obtained by the anodic oxidation can immediately heal the nano-defects, which are on the order of tens to hundreds of nanometers, by combined with oxygen in the defects. Therefore, the anodic oxidation

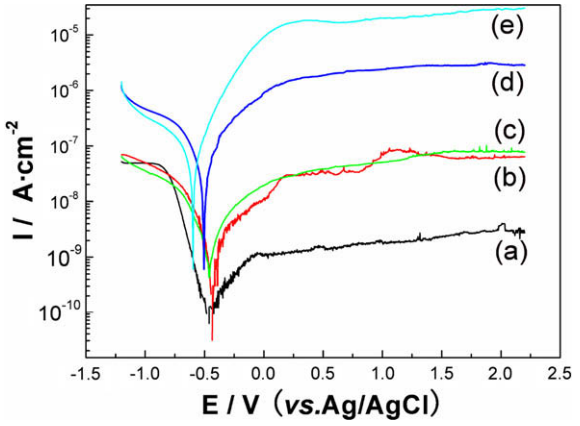

Fig. 5. Polarization curves of the aluminum tabs in ethyeneglycol–borate solution with chloride ions: (a) 0 ppm, (b) 2 ppm, (c) 5 ppm, (d) 50 ppm and (e) 1000 ppm.

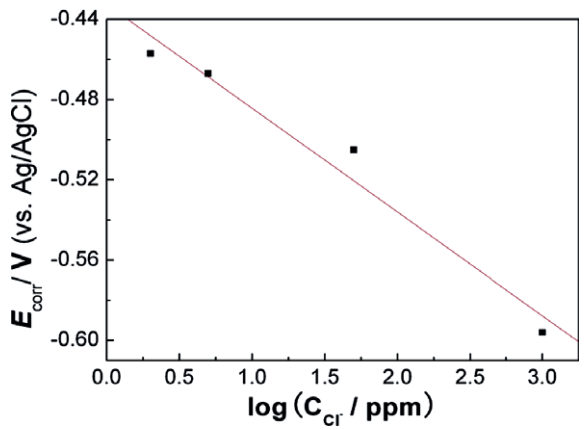

Fig. 6. Dependence of the corrosion potential ($\boldsymbol{E}_{corr}$) on $\log C_{Cl^-}$ for aluminum tabs.

reaction is hindered and the polarization current decline, and thus form a current oscillation. Although the old defect is healed, the new defect is formed by the existing electric tension with potential sweeping. The consecutive current oscillations in the anodic polarization curves are attributed to the repeat process of "defect-self-healing-new defect-reselfhealing". As with the results of AFM images (Fig. 2 a and b), the electrode surface is free of large-scale roughness, and is generally much smoother under oscillatory conditions [29]. The corrosion resistance is better, i.e., the self-healing capacity on the oxide film is better with Cl^- contents lower than 2 ppm.

However, the current oscillation disappeared and the anodic-polarization current increased as the Cl^- concentration increasing (curves c–e in Fig. 5). This phenomenon is ascribed to the Cl^- diffusion in the oxide film of aluminum and the Cl^- ion substitution for partial oxygen site (O-site) [30]. The higher the concentration of Cl^- ions is, the more the Cl^--substitution for O-site in the defect. Some Al^{3+} ions from anodic dissolution react with oxygen to heal the defects, while others react with Cl^- ions to form soluble $AlCl_3$ when anodic oxidation occur at the oxide-film defects. The lower formation rate of Al_2O_3 and the more Cl^--substitution for O-site near the nano-pits make the alumina particle formed during anodic oxidation hardly heal the pit and thus the higher anodic dissolution rate than the self-healing rate. Incomplete self-healing of defects in the oxide film results in the high anodic dissolution rate and incomplete hindering of the anodic oxidation in the defects. Thus, the anodic dissolution is continued at the defects. As a result, the pit width increased (c and d in Fig. 2) and the current oscillation disappeared. Although the anodic polarization current increases with the slower self-healing rate in the higher concentration of Cl^- ions, the factors in the oxide film such as high electric field finally cause the equilibrium between the rate of the anodic oxidation dissolution and that of self-healing with increasing the anodic polarization potential. At last, the polarization current is leveled off with increasing the potential and accordingly the anodic passivation can be detected.

4. Conclusions

The corrosion of the anode tabs in aluminum electrolytic capacitor by Cl^- ion was studied by potentiodynamic polarization, atomic force microscope, scanning electronic microscope and optical microscope measurements. The main conclusions drawn from the studies are:

There were some nano-pits, which are defined as the rectangular pits (β) with a depth less than 55 nm and a width no more than 100 nm in this study, on the oxide film of the anode tabs with the concentration less than or equal to 2 ppm. The nano-pits are healed due to the equilibrium between the rate of Al^{3+} ions produced by anodic oxidation and that of Al_2O_3 formed during anodic oxidation. However, the nano-pits were coalesced into clusters, and accordingly the pitting corrosion of anode tabs is turned into surface corrosion at Cl^- content higher than 2 ppm. This is attributed to the lower formation rate of Al_2O_3 than the dissolution rate of Al^{3+} ions, which is produced form anodic oxidation and partially combines with Cl^- to diffuse into solution. Furthermore, the existence of Cl^- ions widens the crevices on the aluminum oxide film, which is formed by virtue of electric tension during the potential sweeping.

The polarization characteristics are obvious as indicated by the electrochemical response of the anode tabs anodized potentiostatically in ethyleneglycol–borate solution with different concentrations of Cl^- ions. The pronounced current oscillation occurred in the solution with Cl^- ions less than or equal to 2 ppm, and both of the current frequency and amplitude increased with decreasing the Cl^- concentration; while no current oscillation of the anode tabs was observed at Cl^- concentration higher than 2 ppm. The current oscillation is the result of the self-healing ability on the oxide film, the valve-metal characteristic of aluminum, and the filled nano-pits at the Cl^- concentration lower than 2 ppm.

Finally, as derived from the resulting polarization curves, the elevation of Cl^- concentration results in the increase of corrosion current ($\boldsymbol{I}_{corr}$), the negative movement of corrosion potential ($\boldsymbol{E}_{corr}$), the decrease of polarization resistance ($\boldsymbol{R}_p$), and the decline of the cathodic and anodic Tafel slopes (b_c, b_a).

Acknowledgements

We greatly appreciate the support of Jianghai Capacitor Co., Ltd, the National Natural Science Foundation of China for the Key program (20635020), Creative Research Group (20521503), the Transformation of Scientific and Technological Foundation of Jiangsu Province (BA2005029). We also wish to thank graduate student, Zheng-Zhi Yin and Bo Liu, presently at Nanjing University, for their assistances with AFM.

References

[1] A. Nishino, J. Power Sources 60 (1996) 137–147.
[2] R.L. MaSaitis, A.J. Muller, R.L. Opila, L.A. Psota-Kelty, S. Daoud, in: Proceedings-Electronic Components Conference, Characterization and reliability of electrolytic capacitors exposed to halogenated solvents, IEEE, Piscataway, NJ, USA, San Diego, CA, USA, 1992, 611-616.
[3] X.Y. Xu, L. Feng, Electronic Product Reliability and Environmental Testing 5 (2001) 22–26.
[4] H.H. Weatherford, C.W. Brice, Appl. Power Electron. Conference and Exposition, APEC '03. Eighteenth Annu. IEEE, Simulation of industrial AC drive system under fault conditions, 2003, 457–463.
[5] M.L. Gasperi, IEEE T. Ind. Appl. 41 (2005) 1430–1435.
[6] S.G. Parler, IEEE T. Ind. Appl. 39 (2003) 929–935.
[7] M. Hao, W. Linguo, in: W. Linguo (Ed.), Ind. Electron. Soc., IECON, 31st Annu. Conference of IEEE, Fault diagnosis and failure prediction of aluminum electrolytic capacitors in power electronic converters, 2005, 842–847.
[8] R. Alwitt, R. Hills, IEEE T. Parts Mater. Pac. 1 (1965) 28–34.
[9] M.L. Gasperi, Ind. Appl. Conference, 31st IAS Annu. Meeting, IAS '96, IEEE Life prediction model for aluminum electrolytic capacitors, 1996, 1347–1351.
[10] V.A. Sankaran, F.L. Rees, C.S. Avant, in: F.L. Rees (Ed.), Ind. Appl. Conference, 32nd IAS Annu. Meeting, IAS '97, IEEE, Electrolytic capacitor life testing and prediction, 1997, 1058–1065.
[11] A.M. Imam, D.M. Divan, R.G. Harley, T.G. Habetler, in: D.M. Divan (Ed.), Ind. Appl. Conference, 42nd IAS Annu. Meeting IEEE, Electrolytic Capacitor Failure Mechanism Due to Inrush Current, 2007, 730–736.
[12] W.Z. Cao, Y.F. Xia, Electron. Compon. Mater. 10 (1991) 48–51.
[13] B. Melody, The potential for positive tab corrosion in high voltage aluminum electrolytic capacitors caused by electrolytic decomposition products Costa Mesa, Calif. 1993, 199–205.
[14] X.S. Shen, Y.B. Shan, F. Dong, W.D. Chen, M.H. Wei, Z.G. Wang, Electron. Compon. Mater. 13 (1994) 37–40.
[15] T. Martin, K.R. Hebert, J. Electrochem. Soc. 148 (2001) B101–B109.
[16] T.-H. Fang, W.-J. Chang, J. Phys, Chem. Solids 64 (2003) 913–918.
[17] J.A. Richardson, G.C. Wood, Corros. Sci. 10 (1970) 313–323.
[18] C.F. Lin, K.R. Hebert, J. Electrochem. Soc. 137 (1990) 3723–3730.
[19] K. Muthukrishnan, K.R. Hebert, T. Makino, J. Electrochem. Soc. 151 (2004) B340–B346.
[20] V. López, J.A. González, E. Otero, E. Escudero, M. Morcillo, Surf. Coat. Technol. 153 (2002) 235–244.
[21] M. Stern, A.L. Geary, J. Electrochem. Soc. 104 (1957) 56–63.
[22] S.-M. Moon, S.-I. Pyun, Electrochim. Acta 43 (1998) 3117–3126.
[23] G. Moretti, G. Quartarone, A. Tassan, A. Zlngales, Electrochim. Acta 41 (1996) 1971–1980.
[24] L.F. Lin, C.Y. Chao, D.D. Macdonald, J. Electrochem. Soc. 128 (1981) 1194–1198.
[25] H. Masuda, M. Yotsuya, M. Asano, K. Nishio, M. Nakao, A. Yokoo, T. Tamamura, Appl. Phys. Lett. 78 (2001) 826–828.
[26] A.R. Trueman, Corros. Sci. 47 (2005) 2240–2256.
[27] M.A. Amin, S.S. Abd El Rehim, E.E.F. El Sherbini, Electrochim Acta 51 (2006) 4754–4764.
[28] G.T. Burstein, P.C. Pistorius, S.P. Mattin, Corros. Sci. 35 (1993) 57–62.
[29] D.T. Bowlin, A. Scheeline, A.J. Pearlstein, Electrochim. Acta 43 (1998) 417–421.
[30] B.C. Bunker, G.C. Nelson, K.R. Zavadil, J.C. Barbour, F.D. Wall, J.P. Sullivan, C.F. Windisch, M.H. Engelhardt, D.R. Baer, J. Phys. Chem. B 106 (2002) 4705–4713.